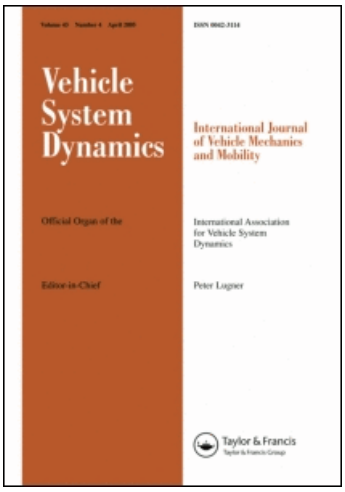

Vehicle System Dynamics
Publication details, including instructions for authors and subscription information:
http://www.informaworld.com/smpp/title~content=t713659010

Impact of inerter nonlinearities on vehicle suspension control

Fu-Cheng Wang [a]; Wei-Jiun Su [a]
[a] Department of Mechanical Engineering, National Taiwan University, Taipei, Republic of China

Online Publication Date: 01 July 2008

To cite this Article Wang, Fu-Cheng and Su, Wei-Jiun(2008)'Impact of inerter nonlinearities on vehicle suspension control',Vehicle System Dynamics,46:7,575 — 595
To link to this Article: DOI: 10.1080/00423110701519031
URL: http://dx.doi.org/10.1080/00423110701519031

Vehicle System Dynamics
Vol. 46, No. 7, July 2008, 575–595

Taylor & Francis
Taylor & Francis Group

Impact of inerter nonlinearities on vehicle suspension control

Fu-Cheng Wang* and Wei-Jiun Su

Department of Mechanical Engineering, National Taiwan University, Taipei, Republic of China

(*Received 1 October 2006; final version received 18 June 2007*)

This paper discusses the nonlinear properties of inerters and their impact on vehicle suspension control. The inerter was recently introduced as an ideal mechanical two-terminal element, which is a substitute for the mass element, where the applied force is proportional to the relative acceleration across the terminals. Until now, ideal inerters have been applied to vehicle, motorcycle and train suspension systems, in which significant performance improvement was achieved. However, due to the mechanical construction, some nonlinear properties of the existing mechanical models of inerters are noted. This paper investigates the inerter nonlinearities, including friction, backlash and the elastic effect, and their influence on vehicle suspension performance. A testing platform is also built to verify the nonlinear properties of the inerter model.

Keywords: inerter; vehicle suspension; performance; nonlinear; optimisation

1. Introduction

The analogy between mechanical and electrical systems is well known. By comparing the dynamic equations, there are two analogies, namely the 'force-voltage' and 'force-current' analogies between the mechanical and electrical networks. In the 'force-current' analogy, the spring, damper and mass of mechanical systems are analogue to the inductor, resistor and capacitor of electrical systems. However, it is noted that one terminal of 'mass' is always grounded, such that the electrical networks with ungrounded capacitors do not have a direct mechanical analogy with springs, dampers and masses. As a result, it potentially narrows the class of passive mechanical impedances that can be physically realised [11]. It was from the appreciation of the gap in the old analogy between mechanical and electrical networks that a new mechanical element, called *inerter*, was proposed [12,14]. An inerter is an ideal mechanical two-terminal element, which is a substitute for the mass element in mechanical/electrical analogy, with the defining equation as follows:

$$F = b\frac{d(v_2 - v_1)}{dt}, \tag{1}$$

*Corresponding author. Email: fcw@ntu.edu.tw

ISSN 0042-3114 print/ISSN 1744-5159 online

DOI: 10.1080/00423110701519031
http://www.informaworld.com

in which F is the applied force and b the inertance of the system, while v_1 and v_2 are the velocities of the two terminals.

With the introduction of inerters, all passive network impedance (admittance) can be mechanically realised by three mechanical elements – springs, dampers and inerters. Consequently, a broader use of passive network impedance (admittance) is allowed to achieve better system performance. The first successful application of the inerter was to vehicle suspension systems [11,13,16], where several layouts of inerters, dampers and springs were optimised for various performance criteria. It was concluded that some layouts are more suitable than others for particular performance criterion. In [9], the optimisation was further carried out by using the Linear Matrix Inequalities method, in which all passive transfer functions with fixed order were optimised for various performance measurements. The resulting passive networks were then synthesised by the Bott–Duffin realisation method. It was shown that the system performance can further be improved by allowing higher-order passive impedance, with the drawback of very complicated network synthesis. The second application of inerter was to the mechanical steering compensator of high-performance motorcycles [2], where the inerter was used to replace a conventional steering damper to stabilise the system in both the 'wobble' and 'weave' modes. The third inerter application was to train suspension systems [17], in which the inerter was located in both the body–bogie and bogie–wheel connections. Significant performance improvement was achieved, especially when employing an inerter between the bogie and the wheel.

Inerters can be mechanically realised in various ways. Until now, two realisations of inerters have been presented [9,11,17]. Due to the mechanical construction, some inerter nonlinearities have been noticed [8,10,11]. In [11], the friction force and damping effect of inerters were noted and used to simulate the frequency responses of a real inerter model. It was pointed out that the experimental data matched better with the theoretical inerter by considering friction forces. In [10], a model was proposed to take the backlash and elastic effect into consideration. The parameters were then adjusted by comparing the time responses of the theoretical and practical inerter models. In [8], a buffer network was placed in series with an inerter to remove the nonlinear spiking of the force signals from the hydraulic testing rig. Through this arrangement, the inerter device behaves as a damper around the crossover frequency and as an ideal inerter in the intermediate frequency range, while at low frequencies it is dominated by friction.

In this paper, a nonlinear inerter model is proposed by considering three nonlinear properties, namely the friction, backlash and elastic effect. Based on the model, we discuss the influence of inerter nonlinearities on vehicle suspension systems. This paper is arranged as follows: in Section 2, three basic suspension layouts are introduced to evaluate the performance of the quarter- and half-car models. In Section 3, a nonlinear inerter model is proposed by considering three nonlinear properties. In Section 4, an experimental platform is built to verify the nonlinearities of a ball-screw inerter model. The parameters of the nonlinear model can be tuned by comparing the experimental and theoretical data. In Sections 5 and 6, nonlinear inerters are applied to vehicle suspension analysis of the quarter- and half-car models. It is shown that the suspension performance is slightly influenced by the inerter nonlinearities. Finally, some conclusions are drawn in Section 7.

2. Vehicle suspension models

In this section, three basic suspension layouts are introduced to evaluate the performance of the quarter- and half-car models.

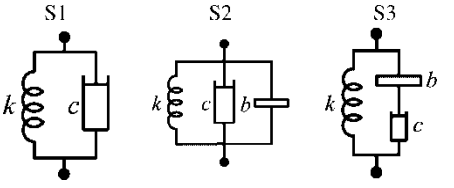

Figure 1. Suspension layouts.

2.1. *Suspension models*

Three kinds of basic suspension layouts, shown in Figure 1, are used for analyses. Among them, S1 is the traditional suspension, while S2 and S3 are suspension models that employ ideal inerters. It is noted that S2 is a basic parallel arrangement and S3 is a basic serial arrangement.

2.2. *Quarter-car model*

A quarter-car model is illustrated in Figure 2, with dynamic equations as follows:

$$m_s \hat{z}_s s^2 = \hat{F}_s - \hat{u}, \tag{2}$$

$$m_u \hat{z}_u s^2 = \hat{u} - \hat{F}_r, \tag{3}$$

where '^' represents the Laplace transform of the corresponding variables, while the tyre force is $\hat{F}_r = k_t(\hat{z}_u - \hat{z}_r)$ and the suspension force u depends on the suspension layouts:

$$\text{For S1,} \quad \hat{u} = (k + c \cdot s)(\hat{z}_s - \hat{z}_u),$$

$$\text{For S2,} \quad \hat{u} = (k + c \cdot s + b \cdot s^2)(\hat{z}_s - \hat{z}_u),$$

$$\text{For S3,} \quad \hat{u} = \left(k + \frac{b \cdot c \cdot s^2}{b \cdot s + c}\right)(\hat{z}_s - \hat{z}_u)\cdot$$

The system transfer function matrix can be represented as

$$\begin{bmatrix} \hat{z}_s \\ \hat{z}_u \end{bmatrix} = G \begin{bmatrix} \hat{F}_s \\ \hat{z}_r \end{bmatrix} = \begin{bmatrix} G_{11} & G_{12} \\ G_{21} & G_{22} \end{bmatrix} \begin{bmatrix} \hat{F}_s \\ \hat{z}_r \end{bmatrix}.$$

To measure the vehicle system performance, three performance indexes are defined as follows [15]:

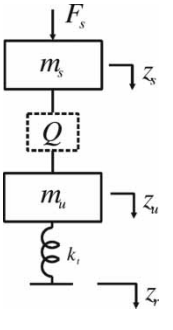

Figure 2. A general quarter-car model.

(1) J_1 (ride comfort)

$$J_1 = 2\pi\sqrt{(V\kappa)}\left\|T_{\hat{z}_r\to\dot{\hat{z}}_s}\right\|_2 = 2\pi\sqrt{(V\kappa)}\left\|sT_{\hat{z}_r\to\hat{z}_s}\right\|_2, \tag{4}$$

where $T_{\hat{z}_r\to\hat{z}_s}$ is G_{12} and $\|sG_{12}\|_2$ is the H_2 norm of the system sG_{12}.

(2) J_3 (dynamic tyre loads)

$$J_3 = 2\pi\sqrt{(V\kappa)}\left\|T_{\dot{\hat{z}}_r\to k_t(\hat{z}_u-\hat{z}_r)}\right\|_2 = 2\pi\sqrt{(V\kappa)}\left\|\frac{1}{s}T_{\hat{z}_r\to k_t(\hat{z}_u-\hat{z}_r)}\right\|_2, \tag{5}$$

where $T_{\hat{z}_r\to k_t(\hat{z}_u-\hat{z}_r)}$ is $k_t(G_{22}-1)$.

(3) J_5 (dynamic load carrying)

$$J_5 = \left\|T_{\hat{F}_s\to\hat{z}_s}\right\|_\infty, \tag{6}$$

where $T_{\hat{F}_s\to\hat{z}_s}$ is G_{11} and $\|G_{11}\|_\infty$ is the H_∞ norm of the system G_{11}.

In equations (4)–(6), V represents the driving velocity, while κ is the road roughness parameter. The parameters are set as $V = 25\,\mathrm{m/s}$ and $\kappa = 5\times10^{-7}\,\mathrm{m^3\,cycle^{-1}}$ for performance analyses. It was shown in [11] that system performance can be improved by adopting inerters into the suspension design. For example, setting the parameters of $m_s = 181.75\,\mathrm{kg}$, $m_u = 25\,\mathrm{kg}$, $k_t = 120\,\mathrm{kN/m}$ [1], J_1 is improved by 13.75% (S2) and 18.74% (S3), and J_3 is improved by 8.28% (S2) and 16.26% (S3), while J_5 is improved by 46.44% (S2) and 33.06% (S3) (Table 1). It is noted that for J_1 and J_3, the achievable performance is better with the serial layout (S3), while for J_5 it is better with the parallel layout (S2).

2.3. *Half-car model*

A half-car model is shown in Figure 3, with dynamic equations as follows:

$$m_s\hat{z}_s s^2 = \hat{F}_s - \hat{u}_f - \hat{u}_r, \tag{7}$$

$$I_\theta\hat{z}_\theta s^2 = \hat{T}_\theta - \hat{u}_f l_f + \hat{u}_r l_r, \tag{8}$$

$$m_{uf}\hat{z}_{uf}s^2 = \hat{u}_f - \hat{F}_{rf}, \tag{9}$$

$$m_{ur}\hat{z}_{ur}s^2 = \hat{u}_r - \hat{F}_{rr} \tag{10}$$

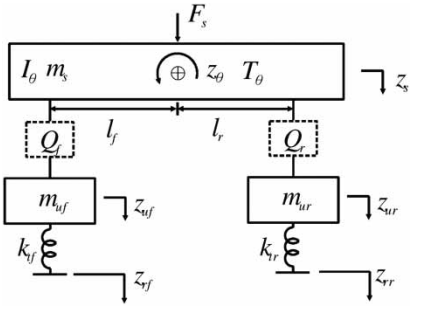

Figure 3. A general half-car model. Subscript f represents the front wheel and r the rear wheel.

where the tyre forces $\hat{F}_{rf} = k_{tf}(\hat{z}_{uf} - \hat{z}_{rf})$, $\hat{F}_{rr} = k_{tr}(\hat{z}_{ur} - \hat{z}_{rr})$, and the suspension force $\hat{\boldsymbol{u}}_{\boldsymbol{i}}$ depends on the suspension layouts:

For S1, $\hat{u}_f = (k_f + c_f s)(\hat{z}_s - \hat{z}_{uf} + l_f\hat{z}_\theta)$, $\quad \hat{u}_r = (k_r + c_r s)(\hat{z}_s - \hat{z}_{ur} - l_r\hat{z}_\theta)$,

For S2, $\hat{u}_f = (k_f + c_f s + b_f s^2)(\hat{z}_s - \hat{z}_{uf} + l_f\hat{z}_\theta)$, $\quad \hat{u}_r = (k_r + c_r s + b_r s^2)(\hat{z}_s - \hat{z}_{ur} - l_r\hat{z}_\theta)$,

For S3, $\hat{u}_f = \left(k_f + \dfrac{b_f c_f s^2}{b_f s + c_f}\right)(\hat{z}_s - \hat{z}_{uf} + l_f\hat{z}_\theta)$, $\quad \hat{u}_r = \left(k_r + \dfrac{b_r c_r s^2}{b_r s + c_r}\right)(\hat{z}_s - \hat{z}_{ur} - l_r\hat{z}_\theta)$,

To analyse the half-car model, the time delay between the front and the rear road disturbances is considered and represented as $\hat{z}_{rr} = \hat{z}_{rf} \cdot \mathrm{e}^{-s\tau}$ with $\tau = L/V$, where L is the wheelbase and V is the forward velocity. Therefore, the system transfer function matrix can be rearranged as follows:

$$\begin{bmatrix}\hat{z}_s & \hat{z}_\theta & \hat{z}_{uf} & \hat{z}_{ur}\end{bmatrix}^T = H\begin{bmatrix}\hat{F}_s & \hat{T}_\theta & \hat{z}_{rf} & \hat{z}_{rr}\end{bmatrix}^T = H'\begin{bmatrix}\hat{F}_s & \hat{T}_\theta & \hat{z}_{rf}\end{bmatrix}^T, \tag{11}$$

in which H is a 4×4 transfer function matrix and H' a 4×3 transfer function matrix. For the analysis of J_1, considering the influence from the pitch angle $\hat{z}_\theta$ to the bounce $\hat{z}_s$ as $\hat{z}_r = (l_f + l_r)\hat{z}_\theta/2$, J_1 of the half-car model is defined as $J_1 = 2\pi\sqrt{V\kappa}(\|sT_{\hat{z}_{rf}\to\hat{z}_s}\|_2 + \|sT_{\hat{z}_{rf}\to\hat{z}_\theta}\|_2)$. Similarly, J_3 of the half-car model is defined as $J_3 = 2\pi\sqrt{V\kappa}(\|(1/(s+a))T_{\hat{z}_{rf}\to k_{tf}(\hat{z}_{uf}-\hat{z}_{rf})}\|_2 + \|(1/(s+a))T_{\hat{z}_{rf}\to k_{tr}(\hat{z}_{ur}-\hat{z}_{rr})}\|_2)$, where $1/s$ in Equation (5) is replaced by $1/(s+a)$ because the transfer functions $T_{\hat{z}_{rf}\to k_{rf}(\hat{z}_{uf}-\hat{z}_{rf})}$ and $T_{\hat{z}_{rf}\to k_{tr}(\hat{z}_{ur}-\hat{z}_{rr})}$ have no zero on the origin. Hence the integral $1/s$ in Equation (5) is multiplied by a high-pass filter $s/(s+a)$ for numerical calculation. Setting $a = 2\pi$(*i.e.* 1 Hz) and $I_\theta = 200\,\mathrm{kgm}^2$, $m_s = 363.5\,\mathrm{kg}$, $m_{uf} = 25\,\mathrm{kg}$, $m_{ur} = 20\,\mathrm{kg}$, $l_f = 0.775\,\mathrm{m}$, $l_r = 1.265\,\mathrm{m}$, $k_{tf} = 120\,\mathrm{kN/m}$, $k_{tr} = 100\,\mathrm{kN/m}$ [1], the performance improvement of the half-car model employing inerters is as follows: J_1 improved by 18.38% (S2) and 19.94% (S3), J_3 improved by 10.78% (S2) and 16.66% (S3), and J_5 improved by 48.82% (S2) and 38.48% (S3) (see Table 2). Similar to the quarter-car analyses, the serial layout (S3) is better for J_1 and J_3, and the parallel layout (S2) is better for J_5.

3. Nonlinearities of inerters

As a mechanical network element, an inerter can be realised in various ways. Until now, two types of inerters have been presented, namely the rack-pinion inerter [11] and the ball-screw inerter [8,17]. However, due to the mechanical construction, the nonlinearities of Inerter models need to be considered [8,10,11]. In this section, three nonlinear properties of a ball-screw inerter, including the backlash, elastic effect and friction, are discussed and a nonlinear inerter model is proposed. Furthermore, a testing platform is introduced to experimentally verify the parameters of the model.

3.1. *Backlash and the elastic effect*

The ball-screw inerter model built by the Mechanical Engineering Department of National Taiwan University (NTU-ME) is illustrated in Figure 4. The working principle of the model is described as follows: two equivalent forces F are applied on the bearing and the nut, such that the screw rotates with the flywheel. When the shaft is twisted by θ, the nut has a translational displacement $x = p(\theta/2\pi)$, where p (in units of m/rev) is the pitch of the screw. Assuming the inertia of the flywheel is I, the ideal inertance of the model is $b = I(2\pi/p)^2$. As in the

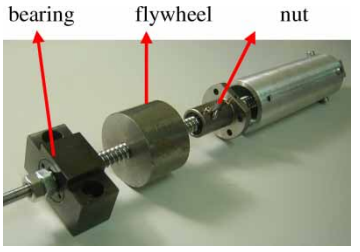

Figure 4. The NTU-ME ball-screw inerter.

backlash and elastic effect of gears shown in [6,10], the backlash ε, the elasticity k_s and viscous damping c_s of the ball-screw inerter can also be considered in the axial direction, as shown in Figure 5.

The dynamic equations of the ball-screw inerter are similar to those of the rotating model in [6]. Considering the displacement x in the axial direction, we define the compressed deformation as $x_s = x_1 - x_3$, the backlash displacement as $x_b = x_3 - x_2$ and the linear displacement between the two ports as $x_d = x_1 - x_2$. Therefore, the corresponding force F can be expressed as:

$$F(t) = k_s x_s + c_s \dot{x}_s = k_s(x_d - x_b) + c_s(\dot{x}_d - \dot{x}_b).$$

In the point of view of contact, three regions are given:

$$A_+ = \{(x_d, \dot{x}_d) \,:\, k_s x_d + c_s \dot{x}_d \geq k_s \varepsilon\},$$
$$A_r = \{(x_d, \dot{x}_d) \,:\, |k_s x_d + c_s \dot{x}_d| < k_s \varepsilon\},$$
$$A_- = \{(x_d, \dot{x}_d) \,:\, k_s x_d + c_s \dot{x}_d \leq -k_s \varepsilon\}.$$

Three contact phenomena can be drawn from [6]:

- There can be persistent right contact (during a non-zero interval) only in A_+ and persistent left contact only in A_-.
- If the system state $(x_d, \dot{x}_d)$ at the initial time $t = t_0$ lies in A_+ with $x_b(t_0) = \varepsilon$ (right contact), then $x_b(t_1) = \varepsilon$ for all times $t_1 > t_0$ such that $(x_d(t), \dot{x}_d(t)) \in A_+$ for all $t \in [t_0, t_1]$. If $(x_d(t_0), \dot{x}_d(t_0)) \in A_-$ with $x_b(t_0) = -\varepsilon$ (left contact), then $x_b(t_1) = -\varepsilon$ for all times $t_1 > t_0$ such that $(x_d(t), \dot{x}_d(t)) \in A_-$ for all $t \in [t_0, t_1]$.
- Assuming that $x_b(t_0) = \varepsilon$ or $x_b(t_0) = -\varepsilon$ and the trajectory $(x_d(t_0), \dot{x}_d(t_0))$ reaches the release set A_r, contact is lost at the first time $t_1 > t_0$.

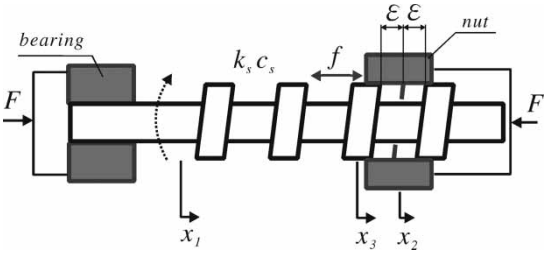

Figure 5. The inerter nonlinearities.

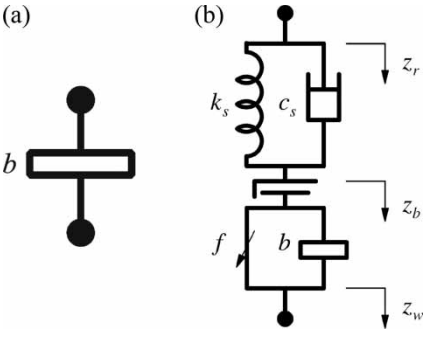

Figure 6. (a) Ideal and (b) nonlinear inerter model.

3.2. *Friction*

Friction force exists in the contact surfaces. In order to reduce the friction, devices are often lubricated to reduce the roughness of the contact surfaces. For the gear motion, friction happens in the contact of the teeth. For the ball-screw, the contact between the nut and screw threads is normally considered as rolling contact with a small friction coefficient [7]. However, for the application of suspension systems, the friction force is not negligible because the normal force on the contact surfaces is significant by preloading.

3.3. *Inerter Model with nonlinear properties*

Considering the aforementioned three nonlinearities, a nonlinear inerter model is proposed in Figure 6b, where c_s and k_s represent the elastic effect, while ε is the backlash and f the friction force.

4. Experimental design and results

In this section, a testing platform is established to verify the proposed nonlinear inerter model.

4.1. *Testing platform*

The testing platform is a motion table that is driven by a servo motor to control the displacement of the suspension strut, as shown in Figure 7 [3,17]. The force of the device is measured by

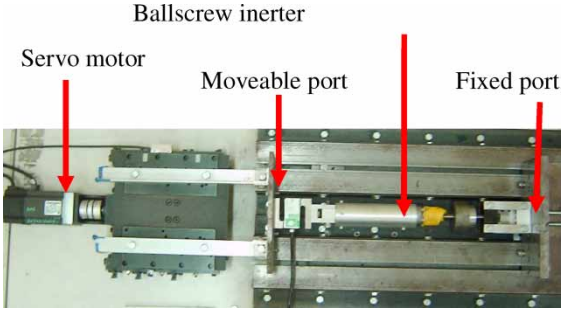

Figure 7. The experimental platform.

an S-type load cell with the maximum load of 100 kg and resolution of 0.02 kg, while the displacement is measured by a position encoder with an accuracy of 1 μm. Both the force and displacement signals are transferred to a LabView™ program to control the movement of the platform and recorded.

4.2. *Theoretical model*

Considering the nonlinear properties, the nonlinear inerter model of Figure 6b is implemented in Simulink™. The simulation results are then compared with the experimental data to tune the corresponding parameters. In the simulations, there are two conditions to be considered, namely the contact condition and the non-contact (backlash) condition, with the dynamic equations as follows:
Contact condition:

$$\boldsymbol{c}_s(\dot{z}_r - \dot{z}_b) + \boldsymbol{k}_s(z_r - z_b) = b(\ddot{z}_b - \ddot{z}_w) + \boldsymbol{f}. \tag{12}$$

Non-contact condition (backlash):

$$\boldsymbol{c}_s(\dot{z}_r - \dot{z}_b) + \boldsymbol{k}_s(z_r - z_b) = 0. \tag{13}$$

4.3. *Parameter settings of the nonlinear inerter*

The parameters of the nonlinear inerter model can be tuned to match the experimental data. The inertance of the ballscrew shaft without the flywheel is 5 kg. A flywheel with corresponding inertance of 108 kg will then be installed for test such that the total inertance is 113 kg. The parameters k_s, c_s, ε and f are tuned using the least-squares steepest descent optimisation algorithm [8] as follows:

$$\min_{k_s, c_s, \varepsilon, f} \|(\boldsymbol{f}_{\text{th}}(\boldsymbol{k}_s, \boldsymbol{c}_s, \varepsilon, \boldsymbol{f}) - \boldsymbol{f}_{\text{exp}})\|_2^2, \tag{14}$$

where f_{exp} is the force measured from the experimental platform and f_{th} is the force calculated from the theoretical nonlinear model.

In order to measure the friction f, the flywheel is uninstalled. The friction force f can then be measured by giving a low-frequency sinusoidal input. Since the inerter force is negligible in this case, the measured force accounts mainly for the friction. Setting the input as a cosine wave of 0.1 Hz with amplitude of 1 mm, the measured displacement and force are shown in Figure 8. It is noted that the friction f is almost a square wave, with the amplitude of 10 N and the direction opposite to the sign of the velocity. So we consider the size of the friction f as constant for the theoretical model such that Equation (12) can be rearranged as:

$$c_s(\dot{z}_r - \dot{z}_b) + k_s(z_r - z_b) = b(\ddot{z}_b - \ddot{z}_w) + f_{\boldsymbol{c}} \cdot \text{sign}(\dot{z}_b - \dot{z}_w), \tag{15}$$

with $f_c = 10$ N.

Given an input $r = \cos(6\pi t)$, the parameters k_s, c_s and ε can be tuned to match the experimental data, as shown in Figure 9. Using the optimisation algorithm of Equation (14), the best fit between the experimental and the theoretical data is taken as follows: $k_s = 1000$ kN/m, $c_s = 3200$ Ns/m and $\varepsilon = 0$.

From the optimisation results, there is no backlash in the ball-screw inerter. The reason is that the ball-screw set is normally preloaded to eliminate the backlash in the manufacturing process [19]. For instance, four preloading methods, namely the double nut preloading, spring preloaded double nut, offset preloading and oversized-ball preloading, are described in [19].

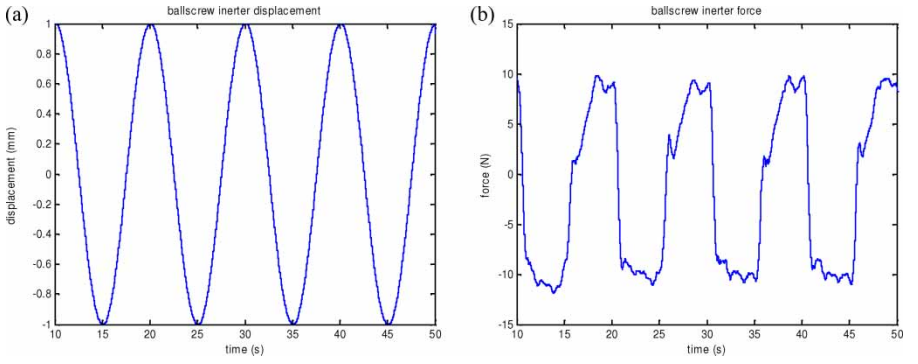

Figure 8. The analyses of inerter friction: (a) displacement, (b) force.

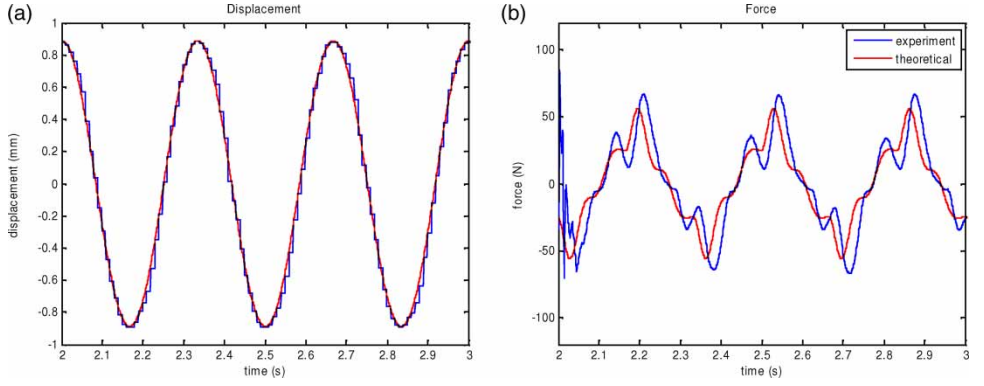

Figure 9. Parameter tuning of the nonlinear inerter model: (a) displacement, (b) force.

4.4. *Frequency-domain responses*

To compare the frequency responses of the experimental and theoretical models, the time-domain data is transformed into the frequency domain using the method illustrated in [Section 6.2, 5]. With parameter settings as follows: $f = 10\,\mathrm{N}$, $k_s = 1000\,\mathrm{kN/m}$, $c_s = 3200\,\mathrm{Ns/m}$, $\varepsilon = 0$ and $b = 113\,\mathrm{kg}$, the frequency responses from the displacement input to the force output are shown in Figure 10. It is illustrated that the theoretical and experimental gains

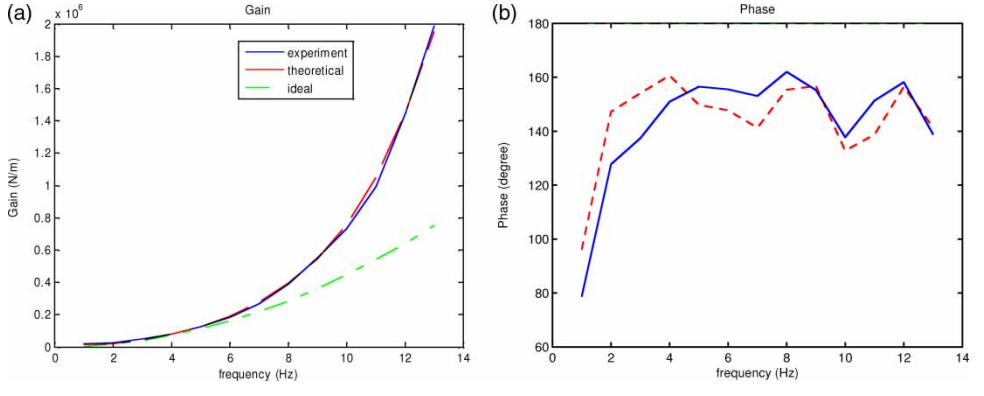

Figure 10. Frequency responses from the displacement input to the force output. (a) Gain plot, (b) Phase plot.

match very well, with little difference in the phase plot. From Figures 9 and 10, it is noted that the theoretical and practical inerter models have similar time- and frequency-domain responses. Therefore, these parameter settings will be used to discuss the impact of inerter nonlinearities on vehicle suspension design in the next sections.

5. The impact of inerter nonlinearities on the suspension design of a quarter-car model

In this section, the nonlinear inerter model is applied to the performance analyses of the quarter-car suspension systems. We consider the three basic suspension layouts of Figure 1, with the linear inerter replaced by the proposed nonlinear inerter model of Figure 6b.

To investigate the performance benefits of the quarter-car model with a nonlinear inerter, three scenarios are discussed to illustrate their individual and combined effects on performance:

- inerter with the elastic effect only,
- inerter with friction only,
- inerter with both friction and the elastic effect.

5.1. *Performance indexes by applying inerter with the elastic effect only*

To consider the influence of the elastic effect, two settings of k_s and c_s are applied to illustrate their impact on suspension performance. The first is from the experimental results of Section 4, where $k_s = 1000\,\text{kN/m}$ and $c_s = 3200\,\text{Ns/m}$. The second is set twice as hard with $k_s = 2000\,\text{kN/m}$ and $c_s = 6400\,\text{Ns/m}$. Referring to Figure 6, an inerter with only the elastic effect can be regarded as a linear model in which an ideal inerter is in series with a parallel spring/damper set, such that the performance optimisation of this model is similar to the linear cases. The optimisation of the performance measures is shown in Figure 11.

For J_1, the performance benefit decreases with the elastic effect, and the performance is degraded more by the softer elastic settings. For J_3, the results are a little different from J_1 optimisation, as shown in Figure 11c and d. For the serial arrangement (S3), the performance improvement is slightly increased when k is less than 120 kN/m. Apart from that, the suspension performance is, in general, degraded by the elastic effect. For J_5, it is noted that the softer shaft has less performance benefits. As illustrated in Figure 11f, the serial arrangement (S3) with elastic effect is even worse than the traditional suspension (S1) when k is about 55 kN/m.

5.2. *Performance indexes by applying inerter with friction only*

In this section, an inerter with friction only is applied to the quarter-car model. Using the nonlinear model described in Section 4.2, two methods are introduced to evaluate the performance of the nonlinear systems.

5.2.1. *Analysis methods*

For linear systems, the performance measures can be evaluated by directly calculating the H_2 and H_∞ norms of the system transfer functions, as shown in Equations (4)–(6). But for nonlinear systems, they can not be directly obtained because the transfer functions are time-varying and depends on the input. For example, considering the backlash of the inerter, the transfer function when it is in the range of backlash is different from the transfer function when

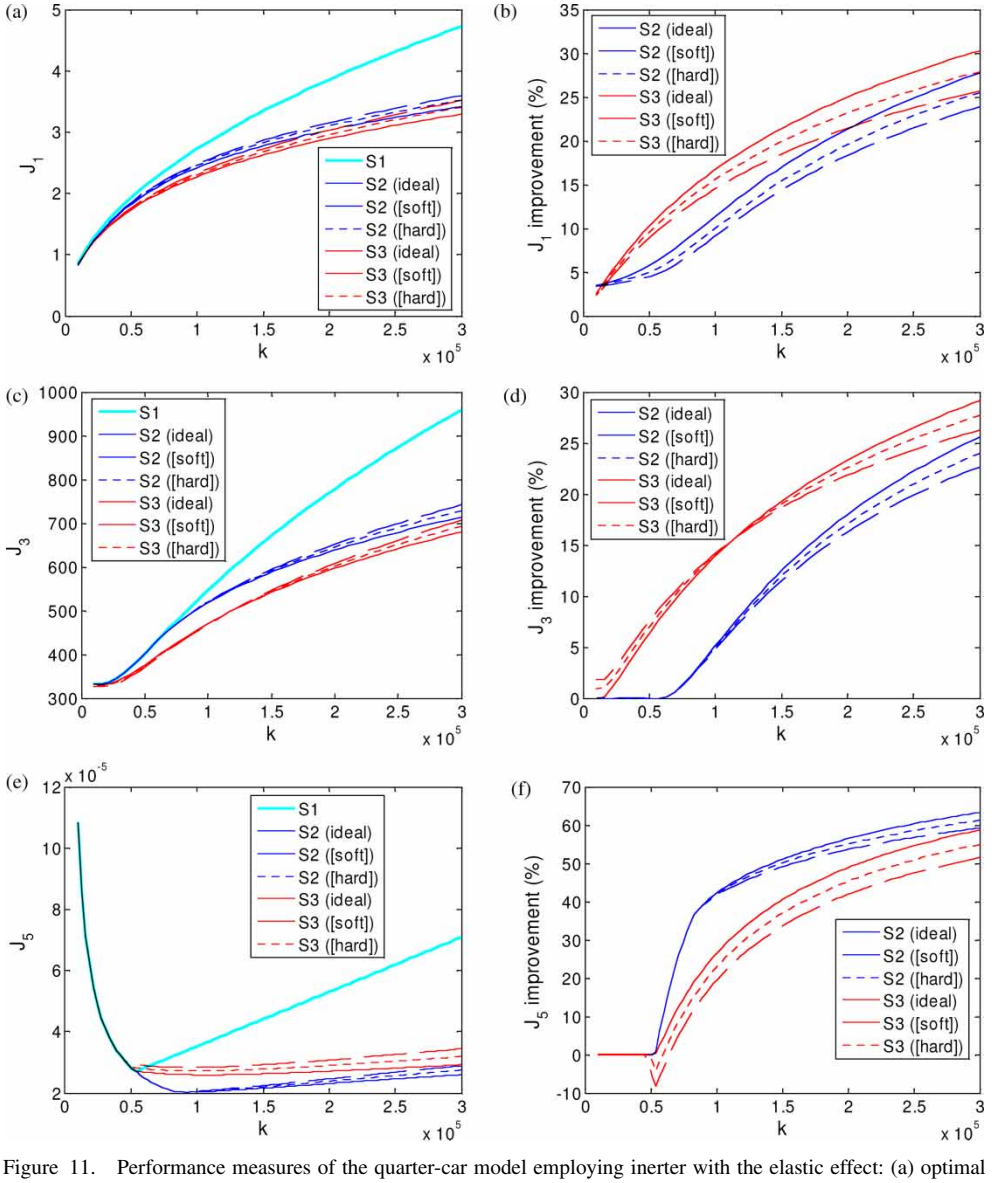

Figure 11. Performance measures of the quarter-car model employing inerter with the elastic effect: (a) optimal J_1, (b) J_1 improvement (%), (c) optimal J_3, (d) J_3 improvement (%), (e) optimal J_5, (f) J_5 improvement (%).

it is in contact. Besides, it is also noted that the performance depends on the input signal. For instance, when the disturbance is large, the suspension displacement and the spring force are also large such that the friction force is relatively negligible. Since there is no backlash in the ball-screw inerter from the experimental results, the analysis will be focused on friction and the elastic effect.

Two methods are proposed to analyse the system performance with a nonlinear inerter. The first is to approximate the nonlinear systems with linear transfer functions at specified frequency such that the system performance can be approximately evaluated by finding the integral and the maximum of system gains in the concerned frequency range. The second is using time-domain responses to measure the performance indexes.

Method 1: approximated linear model method. For the first method, the vehicle model is built in Simulink™. Using a white noise input (z_r or F_s), the input and output time responses are recorded and then transformed into the frequency-domain by fast Fourier transform (FFT). Therefore, at a specified frequency ω_i, the system gains of $|T_{\hat{z}_r \to \hat{z}_s}(j\omega_t)|$, $|T_{\hat{z}_r \to k_t(\hat{z}_u - \hat{z}_r)}(j\omega_i)|$ and $|T_{\hat{F}_s \to \hat{z}_s}(j\omega_i)|$ can be directly calculated by dividing the FFTs of the output and input signals and used to evaluate the performance indexes. Setting the concerned frequency range from 0.01 to 500 Hz, the performance indexes can be approximated by the integral of the system gains (for J_1 and J_3) or by searching for the maximum gain (for J_5) in this range. Furthermore, to verify the accuracy of this method, the performance indexes of linear systems, in which ideal inerters are applied, are also estimated by this method and compared with the direct calculation of system norms. It is shown that the results match each other. Therefore, the performance of nonlinear systems can be estimated by this method.

Input signal. The input signals are set as follows:

- For J_1 and J_3, the input signal is z_r. A white noise of z_r is chosen with the amplitude in the scale of 10 mm. The maximum and the mean absolute values of the signal are set as 13.91 mm and 2.53 mm, respectively, for simulations.
- For J_5, the input signal is F_s. The maximum value of the signal is 1967 N with the mean absolute value of 357.9 N for the quarter-car model. As for the half-car model where the sprung mass is set twice as large as the quarter-car, the input signal F_s is also set twice the size with the maximum value of 3934 N and the mean absolute value of 715.8 N.

Method 2: expected-value method. For the second method, to evaluate performance indexes J_1 and J_3, a suitable input z_r with the spectral density of $S^{z_r}(\boldsymbol{f}) = \kappa \boldsymbol{V}/\boldsymbol{f}^2$ is generated to simulate responses of the nonlinear system [11]. Then the performance indexes are calculated by taking the expected values of the outputs. That is, the *r.m.s. body vertical acceleration discomfort parameter* is $J_1 = \sqrt{E[\ddot{z}_s^2(t)]}$, and the *r.m.s. dynamic tyre load parameter* is $J_3 = \sqrt{(E[F_r^2(t)])}$, in which $F_r = k_t(z_r - z_u)$. It is noted that for linear systems, the expected values equal to the system H_2 norms, *i.e.* $J_1 = \sqrt{(E[\ddot{z}_s^2(t)])} = 2\pi\sqrt{(V\kappa)}\|sT_{\hat{z}_r \to \hat{z}_s}\|_2$, and $J_3 = \sqrt{(E[F_r^2(t)])} = 2\pi\sqrt{(V\kappa)}\|1/sT_{\hat{z}_r \to k_t(\hat{z}_u - \hat{z}_r)}\|_2$, as derived in [11].

To evaluate the performance index J_5, we note that J_5 in Equation (6), which represents the dynamic load carrying, can be regarded as the induced 2-norm of the systems as follows:

$$J_5 = \|T_{\hat{F}_s \to \hat{z}_s}\|_\infty = \sup_{\hat{F}_s \neq 0} \frac{\|\hat{z}_s\|_2}{\|\hat{F}_s\|_2} = \sup_{F_s \neq 0} \frac{\|z_s\|_2}{\|F_s\|_2}, \tag{16}$$

where the last equivalence is from Paseval's relations [18]. That is, the performance index is considered as the maximum ratio of the output energy to the input energy, which can be approximated from the time responses of the system.

Input signal. For J_1 and J_3, the input signal is z_r. Considering the spectral density $S^{z_r}(f) = \kappa \boldsymbol{V}/f^2$ [11], a time sequence

$$z_r = \sum_{i=1}^{N} A_i \sin(\omega_i \boldsymbol{t} + \theta) \tag{17}$$

is generated to represent the input, where N is the number of frequency points. The magnitudes are taken as $\boldsymbol{A}_i = \sqrt{8\pi\kappa \boldsymbol{V} \cdot \Delta\omega_i/\omega_i}$, In which $\Delta\omega_i = \omega_{i+1} - \omega_i$ and $\Delta\omega_N = \Delta\omega_{N-1}$, and the phase θ is random such that the spectral density of z_r is close to $\kappa V/f^2$. In the simulation,

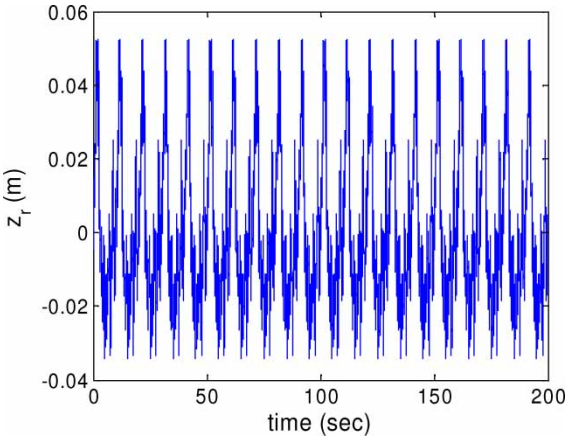

Figure 12. Input signal z_r for the expected-value method.

the frequency points ω_i are set between 0.1 and 1000 Hz with intervals of 0.1 Hz, *i.e.* $\omega_i = [0.1, 0.2, 0.3, \ldots, 1000]$ Hz. An input signal generated from Equation (17) is illustrated in Figure 12. To verify the accuracy of this method, the performance indexes of the linear systems are evaluated by this method and compared with the direct calculation of system norms. The results are shown to match with each other. Therefore, the performance of nonlinear systems can be estimated by this method.

For J_5, the input signal is F_s. First, the peak frequency ω_0 where the infinity norm of the linear system occurs is found. Then, for the nonlinear systems, the input signal is taken as $F_s = A\sin(\omega t)$, in which we set $A = 1000$ N for the quarter-car model and $A = 2000$ N for the half-car model. Then we search the nearby frequency by setting $\omega \approx \omega_0$ to simulate the output responses in order to numerically find the maximum energy ratio by Equation (16).

5.2.2. *Performance indexes by the approximated linear model method*

In order to to illustrate the impact of friction on suspension performance, two settings are applied to the inerter models. The first is $f = 10$ N from the experimental results of Section 4, and the second is twice as big with $f = 20$ N. The optimisation of the performance measures is shown in Figure 13.

For J_1, the results are shown in Figure 13a and b, where the performance benefits are degraded by friction, especially with larger friction. When the suspension stiffness k is small ($k \leq 15$ kN/m), the performance is even worse than the traditional suspension. But when k is large, although the achievable performance is decreased by friction, the overall suspension performance with the frictional inerter is still better than the traditional one (S1). For J_3, the results are similar to J_1, *i.e.* the performance improvement is decreased by friction, as illustrated in Figure 13c and d. When k is small, the performance of S2 and S3 is even worse than the traditional suspension (S1). For J_5, the results are shown in Figure 13e and f where larger friction implies more performance decrease for both S2 and S3 layouts. And, when the system stiffness k is soft, it is shown that S2 with friction is even worse than the traditional suspensions (S1).

5.2.3. *Performance indexes by the expected-value method*

Similarly, to consider the influence of friction on system performance, two settings of $f = 10$ N and $f = 100$ N are applied to the nonlinear simulations. Note that a much larger friction is

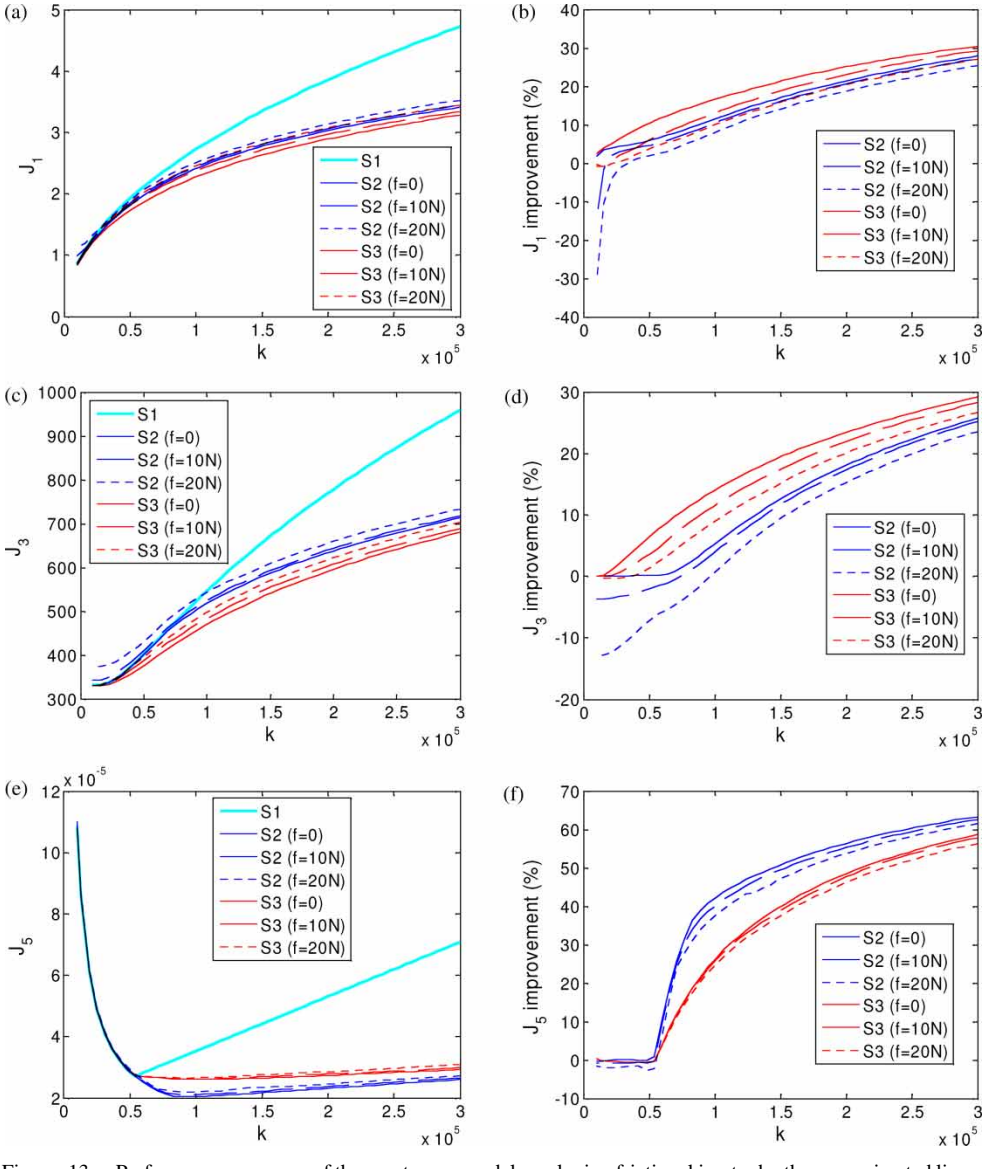

Figure 13. Performance measures of the quarter-car model employing frictional inerter by the approximated linear model method: (a) optimal J_1, (b) J_4 improvement (%), (c) optimal J_3, (d) J_3 improvement (%), (e) optimal J_5, (f) J_5 improvement (%).

set here for comparison, in order to emphasis the impact of inerter friction by this method. Setting the suspension stiffness $k = 120\,\text{kN/m}$, the impact of Inerter friction on performance is illustrated in Table 1, where cases 1, 2, and 7 are with ideal inerters and cases 4, 5, 9 and 10 are with frictional inerters. The expected values of J_1, J_3 and J_5 are taken as the average of four simulations. For accurate comparison, the expected values of the linear models (cases 1, 2 and 7) are compared with the direct calculations of the system norms. It is shown that the errors are within 1%, so the expected value is a reliable performance index.

For J_1, when the friction is small (cases 4 and 9), it is noted that the performance variation is relatively negligible. But when the friction is large (cases 5 and 10), the performance decrease is obvious. For J_3, the influence of friction is similar. When the friction is small (10 N), the

Table 1. Performance measures of the quarter-car model employing inerter with both friction and the elastic effect by the expected-value method ($k = 120\,\text{kN/m}$).

	Case	Layout	c (Ns/m)	b (kg)	J (ideal)	Expectation	Improvement (%)
J_1	1	S1	4981		2.9882	2.9878	
	2	S2	3705.4	128.57	2.5773	2.5885	13.364
	3	S2 (elastic)	3834.4	110.84	2.6488	2.6492	11.332
	4	S2 (friction, $f = 10\,\text{N}$)	3705.4	128.57		2.5878	13.389
	5	S2 (friction, $f = 100\,\text{N}$)	3705.4	128.57		2.6188	12.352
	6	S2 (both)	3834.4	110.84		2.6482	11.366
	7	S3	7544.2	366.52	2.4281	2.4293	18.694
	8	S3 (elastic)	7353	328.72	2.5027	2.5039	16.198
	9	S3 (friction, $f = 10\,\text{N}$)	7544.2	366.52		2.4355	18.485
	10	S3 (friction, $f = 100\,\text{N}$)	7544.2	366.52		2.5000	16.326
	11	S3 (both)	7353	328.72		2.5103	15.981
J_3	1	S1	4674.8		598.52	601.13	0
	2	S2	3933	104.89	548.98	552.07	8.162
	3	S2 (elastic)	3955.8	93.198	552.50	555.54	7.585
	4	S2 (friction, $f = 10\,\text{N}$)	3933	104.89		551.90	8.190
	5	S2 (friction, $f = 100\,\text{N}$)	3933	104.89		557.98	7.179
	6	S2 (both)	3955.8	93.198		555.11	7.657
	7	S3	6666.4	363.55	501.20	504.65	16.050
	8	S3 (elastic)	6736.6	325.42	501.94	505.38	15.929
	9	S3 (friction, $f = 10\,\text{N}$)	6666.4	363.55		506.07	15.815
	10	S3 (friction, $f = 100\,\text{N}$)	6666.4	363.55		519.76	13.537
	11	S3 (both)	6736.6	325.42		506.80	15.692
J_5	1	S1	10230.2		3.8761×10^{-5}	3.8686×10^{-5}	0
	2	S2	9301.3	328.34	2.0761×10^{-5}	2.0736×10^{-5}	46.399
	3	S2 (elastic)	9374.5	271.71	2.1238×10^{-5}	2.1228×10^{-5}	45.127
	4	S2 (friction, $f = 10\,\text{N}$)	9301.3	328.34		2.0848×10^{-5}	46.110
	5	S2 (friction, $f = 100\,\text{N}$)	9301.3	328.34		2.1869×10^{-5}	43.471
	6	S2 (both)	9374.5	271.71		2.1123×10^{-5}	45.399
	7	S3	11174.5	1232.42	2.5946×10^{-5}	2.5924×10^{-5}	32.989
	8	S3 (elastic)	10174.3	888.29	2.8606×10^{-5}	2.8571×10^{-5}	26.146
	9	S3 (friction, $f = 10\,\text{N}$)	11174.5	1232.42		2.5866×10^{-5}	33.139
	10	S3 (friction, $f = 100\,\text{N}$)	11174.5	1232.42		2.5396×10^{-5}	34.354
	11	S3 (both)	10174.3	888.29		2.8584×10^{-5}	26.113

influence on the performance is almost negligible. But when the friction is large (100 N), the performance degrades ~1% for S2 and 2.5% for S3 layouts. To numerically evaluate J_5, the peak frequency at which the linear system achieves infinity norm is found. Then, for the nonlinear systems, an input signal $F_s = A\sin(\omega t)$ with 0 $\omega = \omega_0$ is taken to simulate the output responses in order to find the numerical optimisation for each case of Table 1. For the linear systems (cases 1, 2 and 7), J_5 is calculated from both the theoretical H_∞ norm of Equation (6) and the energy ratio of Equation (16) to illustrate the accuracy of this method. It is shown that the performance is decreased by friction for the parallel arrangement and slightly improved for the serial arrangement. The tendency is more obvious with larger friction settings (cases 5 and 10).

5.3. *Performance indexes by applying inerters with both friction and the elastic effect*

Considering both friction and the elastic effect, a nonlinear inerter model of Figure 6b with the following parameters will be used for analyses: $k_s = 1000\,\text{kN/m}$, $c_s = 3200\,\text{Ns/m}$, $f = 10\,\text{N}$, $\varepsilon = 0$, and c and b the same as the optimal suspensions settings obtained in Section 5.1 (inerter with the elastic effect only).

5.3.1. *Performance indexes by the approximated linear model method*

Using the first method, a nonlinear inerter is applied to the quarter-car model. From the simulation responses, the system gains are obtained at specified frequencies and used to estimate the performance indexes. The results are also compared with the norms of the linear systems. The optimisation results are shown in Figure 14.

For J_1, the optimisation using S2 and S3 are separately illustrated in Figure 14a and b. When k is large, an inerter with only friction is better than an inerter with only the elastic effect. But when k is smaller than 50 kN/m in S2 and 150 kN/m in S3, the result is contrary. And, an inerter with both the elastic effect and friction is always the worst one.

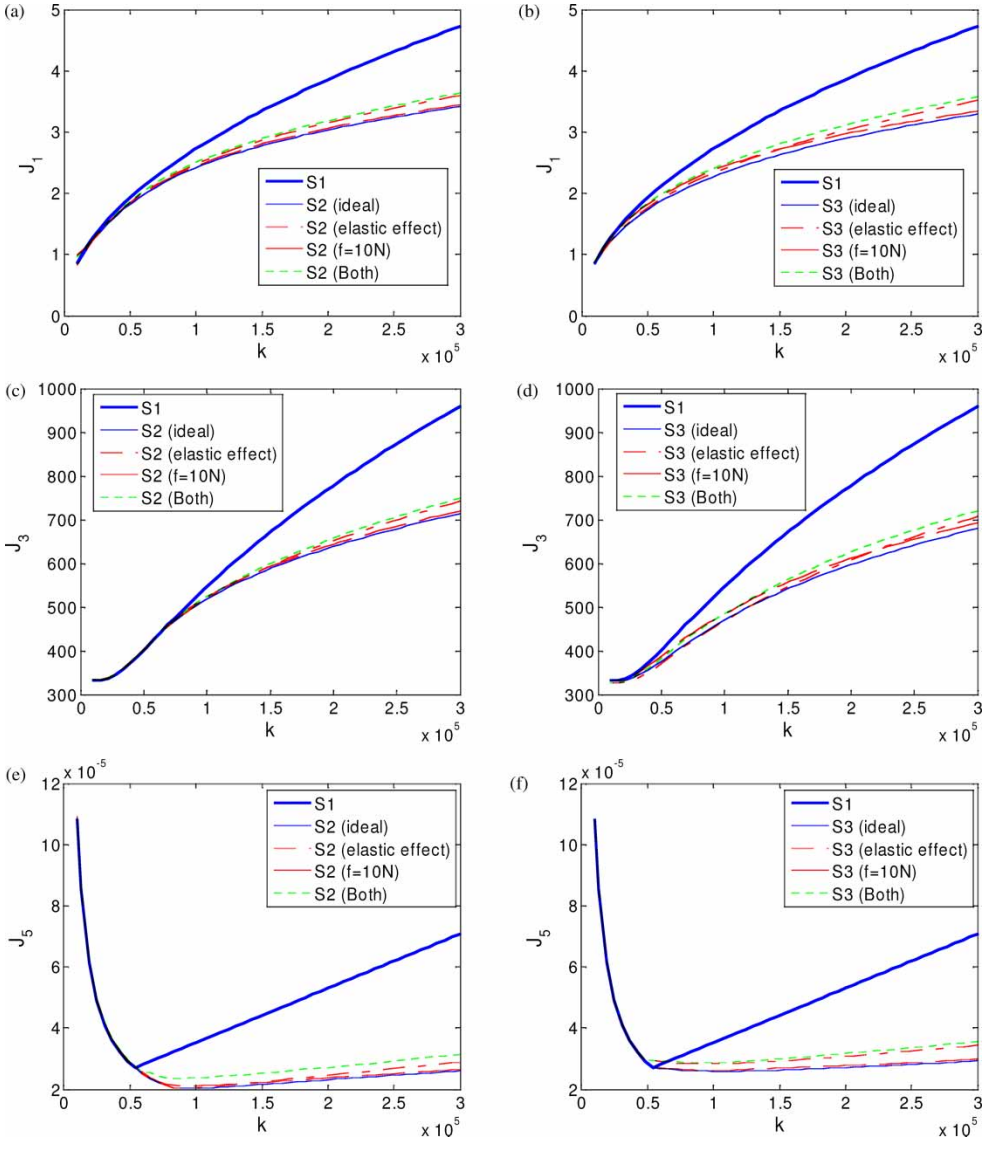

Figure 14. Performance measures of the quarter-car model employing inerter with both friction and elastic effect by the approximated linear model method: (a) optimal J_1 by S2, (b) optimal J_1 by S3, (c) optimal J_3 by S2, (d) optimal J_3 by S3, (e) optimal J_5 by S2, (f) optimal J_5 by S3.

For J_3 analyses, the results are shown in Figure 14c and d, where the serial arrangement (S3) is slightly different from the parallel arrangement (S2). For S2, when k is soft, the ideal inerter is the best one, followed by the inerter with only the elastic effect, the inerter with friction only and the inerter with both friction and the elastic effect. On the other hand, when k is stiffer than 140 kN/m, the ideal inerter is the best one, followed by the inerter with friction only, the inerter with the elastic effect only, and the inerter with both friction and the elastic effect. But for S3, when k is softer than 30 kN/m, the inerter with only the elastic effect is the best one, followed by the inerter with both friction and the elastic effect, the ideal inerter and the inerter with friction only. On the other hand, when k is stiffer than 230 kN/m, the ideal inerter is the best one, followed by the inerter with friction, the inerter with the elastic effect and the inerter with both friction and the elastic effect. That is, J_3 is improved by the elastic effect for the serial arrangement (S3) when k is soft.

For J_5, the results are shown in Figure 14e and f, where the inerter with both the elastic effect and friction is the worst one. For the S3 model, the performance benefit is much more influenced by the elastic effect than friction. For the S2 model, the performance is much influenced by the elastic effect when k is large, while it is much influenced by friction when k is less than 140 kN/m.

We did not discuss the impact of inerter backlash on system performance, not only because the ball-screw model was preloaded to eliminate backlash, but also the weight of the car can be seen as a preloading. That is, even if there is backlash in the inerter model, the inerter should normally remain in the contact condition considering the weight of the vehicle. Therefore, the influence of backlash might be ignored for vehicle applications.

5.3.2. *Performance indexes by the expected-value method*

Using the second method, an inerter with both friction ($f = 10$ N) and the elastic effect ($k_s = 1000$ kN/m and $c_s = 3200$ Ns/m) is applied to the quarter-car model. Similarly, those results are compared with the norms of the linear systems to demonstrate the accuracy of this method. Setting the suspension stiffness $k = 120$ kN/m, the impact of inerter nonlinearities on performance is illustrated in Table 1, where cases 3 and 8 are suspension models with inerters applying the elastic effect only, and cases 6 and 11 are the suspension models with inerters applying both friction and the elastic effect.

For J_1, it is shown that the performance is much more influenced by the elastic effect than friction, and the overall performance is degraded by inerter nonlinearities by 2–3%. For J_3, the influence of inerter nonlinearities is less significant, with the overall degradation of about 0.5%. For J_5, the performance is in general decreased by the elastic effect (cases 3 and 8), but slightly improved by friction for the serial arrangement (S3).

6. Impact of inerter nonlinearities on the suspension design of a half-car model

Similar to the quarter-car model, the performance benefits of inerters for the half-car model are investigated. Setting the suspension stiffness $k_f = k_r = 120$ kN/m, the influence of inerter nonlinearities on suspension performance is illustrated in Tables 2 and 3. In the tables, the optimisation is carried out using several suspension layouts and settings. There are 13 cases in the tables. Case 1 is the traditional suspension. Cases 2 and 8 are the parallel and serial arrangements with an ideal inerter. Cases 3, 4, 9 and 10 are the suspension layouts applying inerters with friction only. Cases 5, 6, 11 and 12 are the suspension layouts applying inerters with the elastic effect only, with $k_s = 1000$ kN/m and $c_s = 3200$ Ns/m in cases 5 and 11, and

$k_s = 2000\,\text{kN/m}$ and $c_s = 6400\,\text{Ns/m}$ in cases 6 and 12. Cases 7 and 13 are the suspension layouts applying inerters with both friction and the elastic effect, in which $k_s = 1000\,\text{kN/m}$, $c_s = 3200\,\text{Ns/m}$ and $f = 10\,\text{N}$.

6.1. *Approximated linear model method*

Using the first method, the nonlinear inerters are implemented to the half-car model to evaluate the performance indexes. The results are shown in Table 2, where the comparing friction force is taken as $f = 20\,\text{N}$ in cases 4 and 10 in order to emphasise the influence of inerter friction.

For J_1, the results are similar to the results of the quarter-car model. First, the performance benefits of an inerter are decreased by both friction and the elastic effect. Second, from cases 2–4 and 8–10, the performance is degraded more by larger friction forces. Third, from cases 5, 6, 11 and 12, the performance is decreased more by softer elastic settings. Finally, the inerter with both friction and the elastic effect is always the worst one.

Table 2. Performance measures of the half-car model by the approximated linear model method ($k = 120\,\text{kN/m}$).

	Case	Layout	J	Improvement (%)	c_f (Ns/m)	c_r (Ns/m)	b_f (kg)	b_r (kg)
J_1	1	S1	6.1101	0	3710.2	4385.6		
	2	S2 (ideal)	4.9873	18.376	2702.3	2852.1	64.15	111.18
	3	S2 ($f = 10\,\text{N}$)	5.0225	17.800	2702.3	2852.1	64.15	111.18
	4	S2 ($f = 20\,\text{N}$)	5.1629	15.502	2702.3	2852.1	64.15	111.18
	5	S2 (soft)	5.1156	16.276	2783.9	2939.5	53.651	96.434
	6	S2 (hard)	5.0575	17.227	2731.8	2896.8	58.551	103.18
	7	S2 ($f = 10\,\text{N}$ + soft)	5.1788	15.242	2783.9	2939.5	53.651	96.434
	8	S3 (ideal)	4.892	19.936	5097.7	7267.2	394.58	227.93
	9	S3 ($f = 10\,\text{N}$)	5.0105	17.996	5097.7	7267.2	394.58	227.93
	10	S3 ($f = 20\,\text{N}$)	5.1595	15.558	5097.7	7267.2	394.58	227.93
	11	S3 (soft)	5.0587	17.208	5108.6	7057.4	366	200.5
	12	S3 (hard)	4.9763	18.556	5104.9	7158	379.91	213.31
	13	S3 ($f = 10\,\text{N}$ + soft)	5.1358	15.946	5108.6	7057.4	366	200.5
J_3	1	S1	1170.5	0	4404.4	4061.2		
	2	S2 (ideal)	1044.3	10.783	4098.7	2939.3	60.441	96.395
	3	S2 ($f = 10\,\text{N}$)	1050.6	10.243	4098.7	2939.3	60.441	96.395
	4	S2 ($f = 20\,\text{N}$)	1073	8.330	4098.7	2939.3	60.441	96.395
	5	S2 (soft)	1053.2	10.021	4119	2976.9	52.561	84.662
	6	S2 (hard)	1048.9	10.389	4109.5	2959	56.231	90.107
	7	S2 ($f = 10\,\text{N}$ + soft)	1060.4	9.406	4119	2976.9	52.561	84.662
	8	S3 (ideal)	975.46	16.660	5849.6	6279.7	456.59	224.47
	9	S3 ($f = 10\,\text{N}$)	1002.6	14.344	5849.6	6279.7	456.59	224.47
	10	S3 ($f = 20\,\text{N}$)	1032.8	11.764	5849.6	6279.7	456.59	224.47
	11	S3 (soft)	982.15	16.091	6091.7	6257.2	414.21	197.37
	12	S3 (hard)	978.6	16.395	5971.9	6269.5	434.36	210
	13	S3 ($f = 10\,\text{N}$ + soft)	1013.1	13.447	6091.7	6257.2	414.21	197.37
J_5	1	S1	2.0532×10^{-5}	0	9666.8	27537		
	2	S2 (ideal)	1.0509×10^{-5}	48.818	8584.8	10322	304.15	1396.8
	3	S2 ($f = 10\,\text{N}$)	1.0843×10^{-5}	47.190	8584.8	10322	304.15	1396.8
	4	S2 ($f = 20\,\text{N}$)	1.1244×10^{-5}	45.237	8584.8	10322	304.15	1396.8
	5	S2 (soft)	1.0939×10^{-5}	46.722	8905.6	9949	247.77	824.16
	6	S2 (hard)	1.0791×10^{-5}	47.443	8357.4	10247	288.54	1092.6
	7	S2 ($f = 10\,\text{N}$ + soft)	1.2238×10^{-5}	40.395	8905.6	9949	247.77	824.16
	8	S3 (ideal)	1.2632×10^{-5}	38.476	10875	57663	1051.1	3720.1
	9	S3 ($f = 10\,\text{N}$)	1.3428×10^{-5}	34.600	10875	57663	1051.1	3720.1
	10	S3 ($f = 20\,\text{N}$)	1.4907×10^{-5}	27.396	10875	57663	1051.1	3720.1
	11	S3 (soft)	1.3954×10^{-5}	32.038	9991.5	64695	785.31	2562.2
	12	S3 (hard)	1.3292×10^{-5}	35.262	10420	56069	899.79	2865.8
	13	S3 ($f = 10\,\text{N}$ + soft)	1.4272×10^{-5}	30.489	9991.5	64695	785.31	2562.2

For J_3, it is noted that the performance is much more influenced by friction than the elastic effect. With a slight increase in friction, the performance is significantly degraded. On the other hand, the performance change is not much when the elastic effect is doubled. Finally, the performance is the worst when considering both the nonlinearities.

The analyses of J_5 suggest that the performance is significantly influenced for the S3 model (cases 9–12), considering either friction or the elastic effect. On the other hand, for the S2 model, the individual influence of inerter nonlinearities is not significant (cases 3–6). However, with both friction and the elastic effect, the overall performance degradation is about 8% for both the S2 and S3 models.

Table 3. Performance measures of the half-car model by the expected-value method ($k = 120\,\text{kN/m}$).

	Case	Layout	c_f (Ns/m)	c_r (Ns/m)	b_f (kg)	b_r (kg)	J	Expectation	Improvement (%)
J_1	1	S1	3710.2	4385.6			6.1101	6.1126	0
	2	S2 (ideal)	2702.3	2852.1	64.15	111.18	4.9873	4.9959	18.269
	3	S2 ($f = 10\,\text{N}$)	2702.3	2852.1	64.15	111.18		4.9943	18.295
	4	S2 ($f = 100\,\text{N}$)	2702.3	2852.1	64.15	111.18		5.0724	17.017
	5	S2 (soft)	2783.9	2939.5	53.651	96.434	5.1156	5.1295	16.082
	6	S2 (hard)	2731.8	2896.8	58.551	103.18	5.0575	5.0715	17.032
	7	S2 ($f = 10\,\text{N} + \text{soft}$)	2783.9	2939.5	53.651	96.434		5.1288	16.095
	8	S3 (ideal)	5097.7	7267.2	394.58	227.93	4.892	4.8981	19.868
	9	S3 ($f = 10\,\text{N}$)	5097.7	7267.2	394.58	227.93		4.9090	19.690
	10	S3 (d N)	5097.7	7267.2	394.58	227.93		5.0320	17.678
	11	S3 (soft)	5108.6	7057.4	366	200.5	5.0587	5.0598	17.223
	12	S3 (hard)	5104.9	7158	379.91	213.31	4.9763	4.9799	18.530
	13	S3 ($f = 10\,\text{N} + \text{soft}$)	5108.6	7057.4	366	200.5		5.0711	17.039
J_3	1	S1	44404.4	4061.2			1170.50	1173.68	0
	2	S2 (ideal)	4098.7	2939.3	60.441	96.395	1044.30	1047.95	10.712
	3	S2 ($f = 10\,\text{N}$)	4098.7	2939.3	60.441	96.395		1047.78	10.727
	4	S2 ($f = 100\,\text{N}$)	4098.7	2939.3	60.441	96.395		1061.75	9.536
	5	S2 (soft)	4119	2976.9	52.561	84.662	1053.20	1056.90	9.950
	6	S2 (hard)	4109.5	2959	56.231	90.107	1048.90	1052.60	10.316
	7	S2 ($f = 10\,\text{N} + \text{soft}$)	4119	2976.9	52.561	84.662		1056.55	9.979
	8	S3 (ideal)	5849.6	6279.7	456.59	224.47	975.46	979.38	16.555
	9	S3 ($f = 10\,\text{N}$)	5849.6	6279.7	456.59	224.47		982.09	16.323
	10	S3 ($f = 100\,\text{N}$)	5849.6	6279.7	456.59	224.47		1009.73	13.969
	11	S3 (soft)	6091.7	6257.2	414.21	197.37	982.15	986.04	15.987
	12	S3 (hard)	5971.9	6269.5	434.36	210	978.60	982.48	16.291
	13	S3 ($f = 10\,\text{N} + \text{soft}$)	6091.7	6257.2	414.21	197.37		988.85	15.748
J_5	1	S1	9666.8	27537			2.0532×10^{-5}	2.0483×10^{-5}	
	2	S2 (ideal)	8584.8	10322	304.15	1396.8	1.0509×10^{-5}	1.0506×10^{-5}	48.709
	3	S2 ($f = 10\,\text{N}$)	8584.8	10322	304.15	1396.8		1.0486×10^{-5}	48.806
	4	S2 ($f = 100\,\text{N}$)	8584.8	10322	304.15	1396.8		1.0948×10^{-5}	46.551
	5	S2 (soft)	8905.6	9949	247.77	824.16	1.0939×10^{-5}	1.0936×10^{-5}	46.609
	6	S2 (hard)	8357.4	10247	288.54	1092.6	1.0791×10^{-5}	1.0777×10^{-5}	47.386
	7	S2 ($f = 10\,\text{N} + \text{soft}$)	8905.6	9949	247.77	824.16		1.0873×10^{-5}	46.917
	8	S3 (ideal)	10875	57663	1051.1	3720.1	1.2632×10^{-5}	1.2598×10^{-5}	38.495
	9	S3 ($f = 10\,\text{N}$)	10875	57663	1051.1	3720.1		1.2599×10^{-5}	38.490
	10	S3 ($f = 100\,\text{N}$)	10875	57663	1051.1	3720.1		1.2593×10^{-5}	38.520
	11	S3 (soft)	9991.5	64695	785.31	2562.2	1.3954×10^{-5}	1.3940×10^{-5}	31.944
	12	S3 (hard)	10420	56069	899.79	2865.8	1.3292×10^{-5}	1.3396×10^{-5}	34.599
	13	S3 ($f = 10\,\text{N} + \text{soft}$)	9991.5	64695	785.31	2562.2		1.3944×10^{-5}	31.924

6.2. *Expected-value method*

Similarly, using the expected-value method, the impact of inerter nonlinearities on the performance of the half-car model is illustrated in Table 3, where the comparing friction force is taken as $f = 100\,\mathrm{N}$ in cases 4 and 10 for emphases.

For J_1, it is shown that the influences of inerter friction are negligible when it is small, where the performance degradation is mainly caused by the elastic effect (cases 3–7 and 9–13). Considering both the nonlinearities, the overall performance is decreased by 2–3%.

For J_3, it is first noted that the influence of friction is negligible unless it is largely increased to $f = 100\,\mathrm{N}$ (cases 3–4 and 9–10). Furthermore, the elastic effect also seems to have little impact on the performance (cases 5–6 and 11–12) at the stiffness setting $k_\mathrm{f} = k_\mathrm{r} = 120\,\mathrm{kN/m}$. The overall performance degradation is less than 1% when considering both of the inerter nonlinearities.

For J_5, the performance degradation is not obvious for the S2 arrangement (cases 2–7), but reaches 6.5% for the S3 arrangement (case 13). Taking the nonlinearities individually, it is shown that the influence is mainly caused by the elastic effect for S3 (cases 11–12), especially for the soft settings.

7. Conclusions

This paper has discussed three nonlinear properties of inerters and proposed a nonlinear inerter model. From the experimental results, it was shown that a ball-screw inerter has both friction and the elastic effect. The nonlinear inerter was then applied to vehicle suspension design. The individual and combined effects of inerter nonlinearities were discussed in three scenarios. Considering the nonlinearities, two analysis methods were proposed to investigate the performance of the suspension systems. From the results, it was noted that the suspension performance was influenced by inerter nonlinearities. In general, the performance benefits of inerters were degraded by considering inerter nonlinearities, except for the S3 model where J_3 was slightly improved by the elastic effect when the suspension stiffness k was small. From the analyses, the performance benefits were slightly degraded by inerter nonlinearities. However, it was illustrated that the overall suspension performance with a nonlinear inerter is still better than the traditional suspensions, especially when the suspension stiffness k is large.

References

[1] J.C. Dixon, *Tyres, Suspension and Handling*, 1st ed., Cambridge University Press, 1991.
[2] S. Evangelou et al., *Steering compensation for high-performance motorcycles*, in *Proceedings of the 43rd IEEE Conference on Decision and Control*, Paradise Island, Bahamas, 14–17 December 2004, pp. 749–754.
[3] M.S. Hsu, *The realisations of inerter concept and the application to building suspension*, Master thesis, National Taiwan University, June 2005.
[4] I.V. Kragelsky, M.N. Dobychin, and V.S. Kombalov, *Friction and Wear calculation methods*, Pergamon Press, 1982.
[5] L. Ljung, *System Identification: Theory for the User*, Prentice-Hall, 1987.
[6] M. Nordin, J. Galic, and P.O. Gutman, *New models for backlash and gear play*, Int. J. Adapt. Control Signal Process. 11 (1997) pp. 49–63.
[7] R.L. Norton, *Machine Design: An integrated Approach*, 2nd ed., Prentice-Hall, 2000, p. 889.
[8] C. Papageorgiou and M.C. Smith, *Laboratory experimental testing of inerters*, in *Proceedings of the 44th IEEE Conference on Decision and Control, 2005 and 2005 European Control Conference*, CDC-ECC '05, 12–15 December 2005, pp. 3351–3356.
[9] C. Papageorgiou and M.C. Smith, *Positive real synthesis using matrix inequalities for mechanical networks: application to vehicle suspension*, IEEE Trans. Control Syst. Technol. 14 (2006), pp. 423–435.
[10] C. Papageorgiou, *Analysis of experimental data from the testing of inerter devices*, Tech. Rep. F-INFENG/TR.524, Department of Engineering, Control Group, University of Cambridge, 2005.

[11] M.C. Smith and F.C. Wang, *Performance benefits in passive vehicle suspensions employing inerters*, Veh. Syst. Dyn. 42(4) (2004), pp. 235–257.
[12] M.C. Smith, *Synthesis of mechanical networks: the inerter*, IEEE Trans. Autom. Control 47 (2002), pp. 1648–1662.
[13] M.C. Smith and F.C. Wang, *Controller parameterization for disturbance response decoupling: application to vehicle active suspension control*, IEEE Trans. Control Syst. Technol. 10 (2002), pp. 393–407.
[14] M.C. Smith, Force-Controlling Mechanical Device, Patent Pending, Intl. App. No. PCT/GB02/03056, Priority Date: 4 July 2001.
[15] M.C. Smith and G.W. Walker, *A mechanical network approach to performance capabilities of passive suspensions*, in: *Proceedings of the Workshop on Modeling and Control of Mechanical Systems*, Imperial College, London, 17–20 June 1997, pp. 103–117, Imperial College Press, London, 1997.
[16] F.C. Wang, *Design and synthesis of active and passive vehicle suspensions*, PhD thesis, Cambridge University, September 2001.
[17] F.C. Wang *et al.* The performance improvements of train *suspension systems with inerters*, in *Proceedings of the 45th IEEE Conference on Decision and Control*, San Diego, USA, 13–15 December 2006, pp. 1472–1477.
[18] K. Zhou, J.C. Doyle, and K. Glover, *Robust and Optimal Control*, Prentice-Hall, 1996.
[19] Catalog of NSK ballscrew, Precision Machine Components, CAT.No.E3161a.